J. Fluid Mech. (2013), *vol.* 735, *pp.* 684–704. © Cambridge University Press 2013
doi:10.1017/jfm.2013.523

Effect of vane thickness on radiometric force

Austin Ventura[1], Natalia Gimelshein[2], Sergey Gimelshein[1,†] and Andrew Ketsdever[1]

[1]University of Colorado – Colorado Springs, Colorado Springs, CO 80918, USA

[2]Gimel, Inc., Montrose, CA 91020, USA

(Received 14 May 2013; revised 23 September 2013; accepted 26 September 2013; first published online 29 October 2013)

A numerical and experimental study of radiometric forces on vanes of different thickness is presented for the flow regime where the radiometric force is near its maximum. For single- and multi-vane geometries, it is shown that radiometric force decreases by only ∼10–15 % when the vane thickness-to-height ratio increases fourfold from 0.5 to 2. For a single-vane geometry, the shear force on the lateral side of the vane is attributed to a vortex flow generated by the interaction of cold chamber walls and heated walls of the vane. In that case, it always acts to reduce the total radiometric force governed by the pressure difference between the hot and the cold sides of the vane. For a multi-vane geometry, represented by a perforated vane, the shear force becomes positive for larger thickness-to-height ratios and lower pressures, primarily due to strong vane-driven transpiration flow through the gaps.

Key words: micro-/nano-fluid dynamics, non-continuum effects, rarefied gas flow

1. Introduction

It has been known since the pioneering work of Crookes (1874) that, if a vane with a temperature gradient over its surface is suspended in rarefied gas, there is a force on that vane produced by gas molecules. The simplest device that uses such a force consists of a planar vane whose sides are kept at different temperatures, most typically through either radiative or resistive heating. The force is usually called radiometric, as the first theories, most notably by Crookes himself, associated that force with radiation origins, and ignored the influence of gas surrounding the vane. Later theories by Reynolds (1874, 1876) and Maxwell (1879) proposed several likely gas-related mechanisms that may contribute to the radiometric force. One of the first and most intuitive theories came from Reynolds (1874), who pointed out that the molecules leave the hotter surface with a larger thermal velocity and, therefore, momentum. The force in highly rarefied gases, when the mean free path is comparable to or larger than the vane size, is thus caused by a difference in the momentum flux of the molecules leaving the hot surface and the cold surface. Such a force, which acts in the direction from the hot to cold side of the vane, depends on the vane area, and is generally called the area force.

At about the same time as Reynolds, Maxwell (1879) also showed that an unbalanced force exists near the edge of the hot side of the vane, where the heat

† Email address for correspondence: gimelshe@usc.edu

https://doi.org/10.1017/jfm.2013.523 Published online by Cambridge University Press

flow in the gas is non-uniform. Almost fifty years later, Einstein (1924) presented a simple theory, according to which the force exerted on the vane is proportional to its perimeter. This edge dependence of the vane force has found partial confirmation in the experimental work of Marsh (1926), where the force was shown to depend on perimeter, although the dependence is weaker than Einstein's prediction. The edge force is generally produced within a few mean free paths of the vane's edge and is the dominant force at low Knudsen numbers. Thermal stresses in the gas surrounding the edge are the main reason for this force, as shown by Taguchi & Aoki (2012). The temperature gradient along the edge of the radiometer vane sets up tangential stresses on the vane driven by the process of thermal creep. Thermal creep is a transitional flow regime phenomenon where the flow moves from the cold vane surface to the hot surface. Thermal creep may be partially responsible for a pressure difference near the edge of a radiometer vane that sets up a larger pressure on the hot side than the cold side contributing to a force near the edge. The edge force related to this mechanism, similar to the area force, acts in a direction from the hot to cold surfaces.

The third gas-driven mechanism that contributes to the radiometric force is related to the finite thickness of a radiometer vane. That third mechanism discussed by Reynolds (1876) is the shear force, which is also produced by thermal creep. While the relative importance of the area and edge forces is primarily determined by the vane length-based Knudsen number, Kn, with the area force dominating for Kn greater than ~ 0.1 and the edge force becoming more important for smaller Kn, the shear force is expected to be impacted also by the vane thickness. Generally, the shear force that acts on the lateral edge of the vane is expected to become noticeable at low Knudsen numbers, $Kn < 0.1$, provided the thickness is non-negligible. Thus, the net force acting on the radiometer vane is a balance between the area and edge forces and the shear. The area and edge effects are responsible for the direction of rotation of the vanes in a Crookes radiometer with the hot, darkened surfaces trailing the cold, reflective surfaces. Early expressions for the radiometric force range from the functional dependence of the force on gas pressure that captures its bell shape, presented by Brüche & Littwin (1928), to perimeter-based expressions of Einstein (1924) and Sexl (1926), to the area-based force expression of Czerny & Hettner (1924) that connects the force to the thermal creep.

More recently, an analytic expression for the radiometric force was derived by Scandurra, Iacopetti & Colona (2007) that has both pressure and shear components. The shear, often ignored in earlier studies, is produced by the interaction of gas with the lateral surface of the vane. The results of Scandurra *et al.* (2007) predicted the shear force to act from the hot to the cold side, thus increasing the total radiometric force. This finding directly contradicts the numerical results obtained by different kinetic approaches (see Selden *et al.* 2009*a*,*b*; ?). The direct simulation Monte Carlo (DSMC) method, the numerical solution of the model kinetic equations, and the combined ellipsoidal statistical Bhatnagar–Gross–Krook/direct simulation Monte Carlo (ES-BGK/DSMC) approach all showed that the shear force on a rectangular radiometer would decrease the total force.

Either positive (Scandurra *et al.* 2007) or negative (Selden *et al.* 2009*a*), the shear force is expected to be noticeably smaller than the pressure force on the working side of the radiometer, assuming that the radiometer is sufficiently thin. For a thin vane geometry, the shear force is expected to be noticeably smaller than the area and the edge forces exerted on the working sides of the radiometer (Selden *et al.* 2009*c*), although its contribution is expected to grow with gas pressure. However, the actual role of shear in thick vane geometries is largely unknown, even though it may play the

https://doi.org/10.1017/jfm.2013.523 Published online by Cambridge University Press

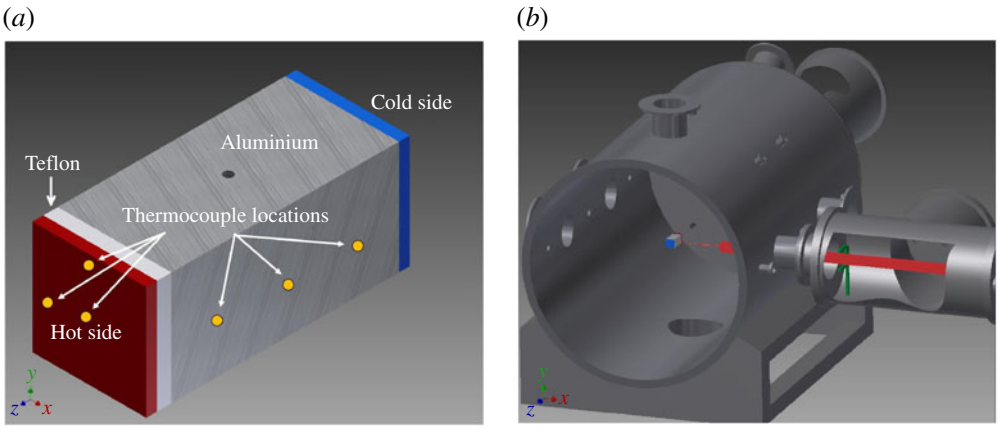


FIGURE 1. (Colour online) (*a*) Radiometric vane construction. (*b*) Schematic of the experimental set-up.

key role in some cases. One example is for multi-vane configurations, where the vanes are closely packed and there is transpiration flow between the cold and hot sides of the radiometer. It has been shown by Cornella *et al.* (2012) that multi-vane radiometers have a much higher ratio of radiometric force to vane mass for a given total area occupied by the radiometer. However, the shear force that is inherently present in such configurations, especially at the microscale where the vane thickness-to-length ratio may easily be larger than unity, may strongly affect the efficiency of such devices. The main objective of this work is to provide experimental and numerical analysis of the shear force produced by the lateral sides of a radiometric vane, and estimate the effect of vane thickness and gas pressure.

2. Experimental set-up

The radiometer vanes for this work, schematically illustrated in figure 1(*a*), were composed of two commercially available thermoelectric coolers, an insulating piece of Teflon and a machined aluminium block. The thermoelectric coolers are composed of two ceramic plates connected with a grid of semiconductors. They measure 40 mm $\times$ 40 mm with a thickness of 3.4 mm. For each set-up, the length of the aluminium block was varied, with lengths of 20, 40 and 80 mm. The Teflon plates were attached between the hot thermoelectric cooler and the aluminium block to limit heat transfer to the aluminium, thereby setting up a thermal gradient along the lateral surfaces. The Teflon plates were 40 mm $\times$ 40 mm and 5 mm thick. The total lengths of the assemblies are 32.1, 51.4 and 91.8 mm, respectively. The thermoelectric cooler on the back of the assembly was not actively heated, making it the cold side of the vane.

The experiment was conducted in a 1 m diameter by 2 m cylindrical vacuum chamber. The chamber had an extension on the side to house a nano-newton thrust stand (nNTS). Details of the nNTS system can be found in Jamison, Ketsdever & Muntz (2002). The radiometers for the experiment were suspended on the end of the thrust stand so that they hung over the centre line of the main chamber. The chamber was pumped down to 10^{-5} Torr using a turbomolecular pump. Before each test was conducted, the vacuum chamber was allowed to sit at vacuum overnight to reduce

https://doi.org/10.1017/jfm.2013.523 Published online by Cambridge University Press

outgassing during the experiment. Figure 1(*b*) shows the shear vane attached to the nNTS in the chamber.

Each of the assemblies was characterized at input powers ranging from 0.25 to 1 W. For characterization, three J-type thermocouples were attached to both vane faces along with a length-dependent number of thermocouples attached to the aluminium surface. Each input power was characterized to have a specific temperature difference between the hot and cold faces. In order to replicate the conditions experienced by the vanes during testing, the thermal characterization was also performed with chamber pressures at the maximum expected pressure for the experiment. This test confirmed that the temperature gradients across the vane remained unchanged while interacting with the working fluid for the experiment. This process was completed long before thrust data were taken, so adsorbing gas on the vanes from the characterization would not have affected the thrust data. Since all thrust data were taken with gas in the chamber, adsorbing and outgassing could have occurred during the experiment. The experimental set-up was always allowed to sit at vacuum overnight between tests to limit the impact of outgassing. The flow caused a uniform cooling on both faces of the assembly, lowering the absolute temperatures by less than 2 K but ultimately not changing the temperature difference, ΔT. The temperature on the surface of the aluminium block exceeded the temperature of the cold side of the assembly by more than 0.5 K for the input powers used in this experiment. The blocks were tested at a ΔT of 23 and 32 K. Note that the thermal characterization revealed no temperature gradient on the vane faces within the specified error of the thermocouples.

The thrust stand was calibrated each day before thrust data were taken using an electrostatic comb calibration system (ESCCS). Details of this calibration method can be found in Selden & Ketsdever (2003). After calibration, argon gas was flowed into the chamber to create steady-state pressures in the chamber. This pressure was varied between 0.1 and 3.25 Pa. After the thrust stand had reached steady-state deflection, the displacement of the stand was measured using a linear variable differential transformer (LVDT). The deflection was used to find the force produced at each pressure. Three separate force measurements were taken at each pressure. The stand position was also measured before and after each gas flow to establish a zero for the stand. The end result of this procedure was a force versus chamber pressure graph that was curve-fitted. The maximum of the generated curve-fitted line was used as the maximum force value for each radiometer at each input power.

3. Numerical approach

Numerical modelling of radiometric phenomena encounters a number of physical and computational challenges, primarily related to the surface-driven, non-equilibrium, subsonic ($M \ll 1$) nature of the associated flows. The dominating role of thermal stresses in the radiometric forces make conventional computational fluid dynamics (CFD) approaches, such as those based on the solution of Navier–Stokes equation, inapplicable. Continuum approaches based on higher moments, such as the 13 moment equations (see e.g. Young 2011), may generally be used only for a first-order estimate of the integral force, and are applicable only for Knudsen numbers smaller than one. The only way to obtain physically accurate solutions in the flow regimes from free molecular to near-continuum is to use computational methods of the kinetic gas theory, and solve the Boltzmann equation or one of its approximations.

Various approaches to the solution of the Boltzmann equation, both fully stochastic, such as the DSMC method of Bird (1994), or mostly deterministic, such as the direct

https://doi.org/10.1017/jfm.2013.523 Published online by Cambridge University Press

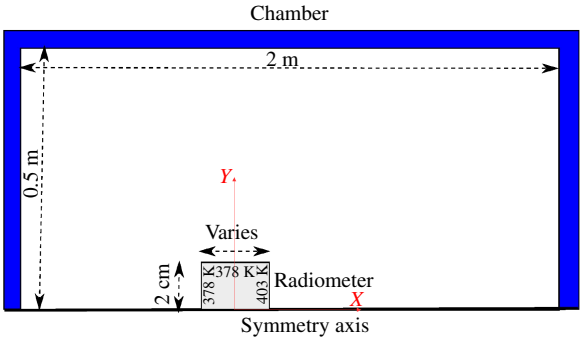


FIGURE 2. (Colour online) Computational set-up.

numerical integration of the Boltzmann equation proposed by Tcheremissine (1996), become prohibitively computationally expensive even for two-dimensional or axially symmetric radiometric set-ups. The primary reason is the characteristically long time to reach steady state, and thus extremely large numbers of time steps are required for explicit time stepping schemes. For a stochastic approach, very low signal-to-noise ratios are present. Radiometric forces typically amount to a fraction of one per cent of a pressure force on a comparable surface at any given pressure, and the flow velocities are usually in the centimetre per second range, as compared to the molecular thermal velocities of the order of 500 m s^{-1}. A plausible alternative is to consider a kinetic approximation of the Boltzmann equation, such as the BGK model or the ES model of Holway (1966), and apply an implicit scheme in time.

In this work, an implicit/explicit finite volume solver (SMOKE) developed by Gimelshein *et al.* (2010) has been used to deterministically solve the ES kinetic equation. The benefit of using the ES equation is its ability to capture the correct Prandtl number, and the proven H-theorem for this equation. SMOKE is a parallel code based on time-implicit and -explicit conservative numerical schemes developed by Mieussens (2000). The geometric set-up is illustrated in figure 2. Note that a full three-dimensional model for the chosen geometrical set-up is not possible, since it would require a prohibitive amount of computer time (up to a year on a modern thousand-processor computer). Using a smaller domain or a coarse three-dimensional grid would unpredictably skew the results, as shown by Selden *et al.* (2009*b*). Therefore, the axially symmetric/two-dimensional capability of SMOKE has been used in this work. For the parameters under consideration, the axisymmetric set-up provides the closest possible match to the described experimental set-up. The two-dimensional set-up provides a useful extrapolation to a long vane configuration that was not possible to measure experimentally. Note that the previous experimental effort of Selden *et al.* (2009*c*), where the measurements were conducted for relatively thin radiometer vanes of different shapes, which include rectangles and a circle, showed that the qualitative behaviour of the total radiometric force as a function of pressure does not depend on the shape, and the maximum force of a rectangle differs from that on a circle by less than 10 %, provided they have the same area.

The vane diameter D (height in two dimensions) was 40 mm in all computations, and the thickness L varied from $L/D = 0.08$ to $L/D = 2$ in order to study the effect of the shear. Here, D is the vane diameter (or vane height for two dimensions). A second-order spatial discretization is used along with implicit time integration. A

https://doi.org/10.1017/jfm.2013.523 Published online by Cambridge University Press

symmetry plane (symmetry axis in axisymmetric computations) was set at the lower boundary. Fully diffuse reflection with complete energy accommodation is applied at the vane and chamber walls. Although it is known that the accommodation coefficient depends on gas and surface material properties, as well as temperatures, and its choice was shown to impact the magnitude of radiometric force in Selden *et al.* (2009*a*), a change in accommodation coefficient is not expected to qualitatively change the dependence of gas flow and forces on the vane geometry examined in this work. In addition, the accommodation coefficient for argon on metals at temperatures near the room level are between 0.8 and 0.9, and thus is close to the fully diffuse value of 1. The selected hot and wall temperatures were those close to the experimental conditions, and the temperature difference $\Delta T = T_{hot} - T_{cold} = 25$ K is small enough so that the radiometric force F is linear with ΔT. Thus the numerical values of $F/\Delta T$ may be directly compared to the measurements.

Two temperature conditions were tested at the lateral wall: a uniform $T = 378$ K, pictured in figure 2; and a linear gradient from $T = 378$ K near the cold side to $T = 403$ K near the hot side. Hereafter, these temperature conditions are labelled TC1 and TC2, respectively. In order to examine the impact of the thermal creep flow driven by the cold chamber walls, additional computations were conducted for $T_{cold} = T_{chamber} = 300$ K, with the same ΔT of 25 K, and a linear temperature gradient at the lateral wall. This temperature case, called TC3 hereafter, corresponds to the case of a perfect insulator between the sides of the radiometer.

The test gas was argon in all cases, and gas pressure ranged from 0.5 to 2.5 Pa to provide the Knudsen number variation between 0.3 and 0.06, and thus cover the flow regime where the radiometric force is near its maximum. Here, the Knudsen number is calculated as the ratio of the gas mean free path in the free stream (undisturbed flow far from the radiometer) to the diameter (height) of the vane. The gas mean free path is evaluated with a variable hard-sphere/variable soft-sphere (VHS/VSS) model expression that may be found in Bird (1994). The grid convergence was achieved by increasing the number of spatial nodes and points in the velocity space. The latter one was (18, 18, 12) for the results presented below, and the number of spatial cells varied between 40 000 and 80 000. The radiometric force on the vane was calculated through the integration of the velocity distribution functions of the incoming and outgoing molecules. Both the normal component of molecular velocities on the working (vertical) sides of the vane (pressure force, F_p) and the tangential component of velocities on the lateral (horizontal) side of the vane (shear force, F_s) contribute to the total radiometric force, F_t.

4. Flow over a single vane: analysis of gas parameters

The representative structure of the gas flow inside the chamber is illustrated in figure 3, where the gas temperature and flow streamlines are plotted for two-dimensional (the vane is a plate infinitely long in the Z direction) and axisymmetric (the vane is a cylinder) configurations for a Knudsen number, Kn, of 0.5. Note that the axisymmetric (AS) field is mirrored with respect to the X axis to provide an easier comparison. The most important conclusion from the flow field is that for two-dimensional flow the impact of the vane is much more significant. Near the chamber walls the gas temperature is $\sim$1 K higher than the chamber temperature $T_w = 300$ K. That means that the flow near the vane, and the radiometric force in particular, is affected by the chamber size. In the axially symmetric flow simulation, and probably in the experiments as well, the gas essentially equilibrates with the

https://doi.org/10.1017/jfm.2013.523 Published online by Cambridge University Press

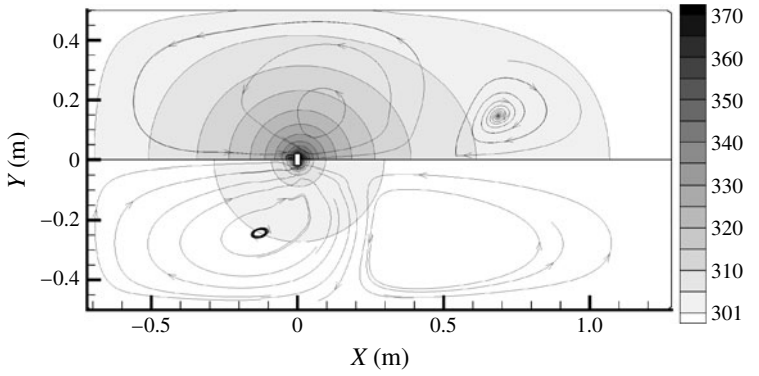


FIGURE 3. Two-dimensional (upper half) and axisymmetric (lower half) flow field structure. Streamlines and temperature fields for $L/D = 0.5$, $p_0 = 0.5$ Pa and TC2. Insets: the corresponding zoomed-in flows near the vane.

chamber wall, as its temperature is only of the order of 0.01 K higher than T_w. The AS radiometric force results are, therefore, virtually free of any chamber wall effect. This was implicitly confirmed in our chamber size convergence study (not shown here), where the radiometric force computed in an almost three times smaller chamber was found to be only a few per cent larger than the baseline results. The dominant effect of chamber walls in the two-dimensional flow, and their relatively small impact in axially symmetric geometry, result in noticeably different flow patterns for these two cases. As will be shown below, this difference may be to a large extent attributed to the thermal creep flow between cold chamber walls and heated surfaces of the vane. Such thermal creep flow is weaker for the AS configuration.

The temperature fields show that, as expected, there is a significant temperature jump at the vane surface for the relatively low Knudsen number, which amounts to about a 30 K jump for the two-dimensional case and over a 40 K jump for the AS case. The larger temperature jump for the latter is due to a larger proportion of colder molecules that move from the periphery, where the temperature is lower, to the vane, as compared to the two-dimensional case. The streamlines, also given in figure 3, illustrate a fairly complex vortex structure for the chosen radiometric set-up. Generally, one can expect a transpiration-type flow Kennard (1938) that moves gas from colder to warmer regions. In the flow presented here, there are three types of possible transpiration: (i) flow from the cold to the hot side of the vane; (ii) flow from the cold chamber walls to the cold side of the vane (which is still much hotter than the chamber, 378 versus 300 K); and (iii) flow from chamber walls to the hot side of the vane. As will be discussed below, the specific vortex structure changes with the temperature regime and vane thickness. In the results presented in figure 3 for the two-dimensional case, the dominant flow is from the chamber walls to the hot side of the vanes, causing the formation of a large vortex, which covers most of the chamber. There is also a small vortex at the cold side of the vane, and a weak but relatively large vortex in the right half of the chamber. In the AS flow, the impact of the chamber walls is smaller, and the strongest vortex mechanism is transpiration from the cold to the hot sides of the vane. For thicker AS vanes, though, the chamber walls play a bigger role, as will be shown below.

The single most important property in radiometric flows is usually the radiometric force, and the gas flow properties that govern the force are gas pressure and flow

https://doi.org/10.1017/jfm.2013.523 Published online by Cambridge University Press

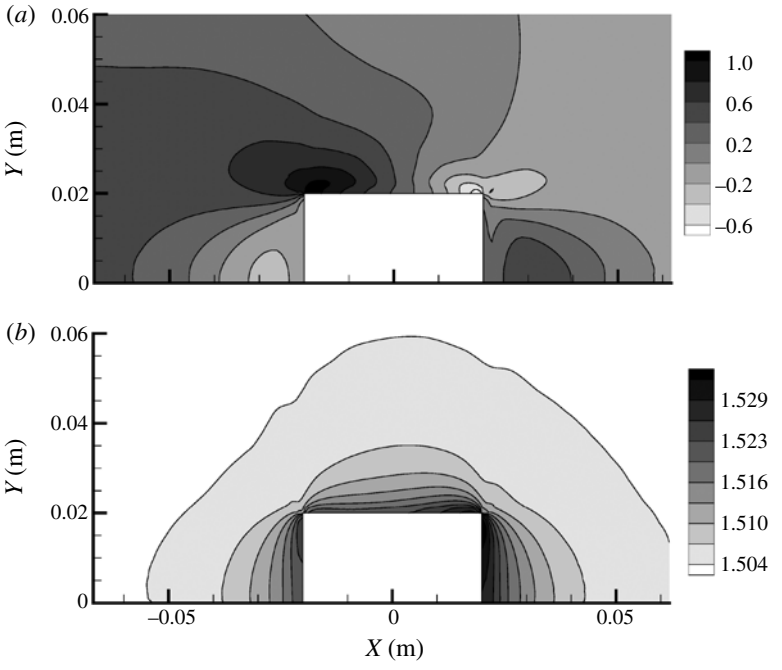


FIGURE 4. Radiometric force contributors: (*a*) velocity in X direction and (*b*) pressure fields over an axisymmetric radiometer for $L/D = 1$, $p_0 = 1.5$ Pa and TC2.

velocity in the direction of the force (X direction in the figures). They are presented in figure 4 for a thicker vane and higher gas pressure. Only a small portion of the computational domain is shown to provide better detail in the vicinity of the vane. At a distance of one mean free path (∼4 mm) away from the hot and cold sides of the vane, the average flow velocities are of the order of -0.2 and 0.2 m s^{-1}, respectively. They are expected to balance each other and should not be a significant contributor to the radiometric force. The flow over the sidewall of the vane is mostly from cold to hot (left to right), although there is a visible region with negative velocities near the hot edge of the vane. Still, the left-to-right flow (hot to cold) largely dominates, and reaches 1 m s^{-1} near the cold edge. Note that, if the vane were the only source of the bulk flow velocity, then from Newton's third law one would expect the bulk flow-related shear force to be directed from right to left, opposite to the flow motion. However, the key player in the bulk flow generation in this case is the chamber wall, and thus that force is in fact directed opposite to the total radiometric force that acts from hot to cold.

The flow velocity in the axial direction is mostly negative, hot to cold, near the cold side of the vane (of the order of -0.2 m s^{-1} one mean free path away from the surface), and positive near the hot side (of the order of 0.3 m s^{-1}), as shown in figure 4(*a*). Note that the magnitude of the drag force on a disk immersed in a subsonic flow may be evaluated as $F_d = 0.5\rho U^2 r^2 C_D$, where ρ and U are gas density and velocity, respectively, r is the disk radius, and C_D is the drag coefficient calculated as $C_D = (64/\pi Re)(1 + (Re/2\pi))$ for $Re < 0.01$ (Clift, Grace & Weber 1978). The Reynolds number for an argon pressure of 1.5 Pa, density of 2.44×10^{-5} kg m^{-3} and flow velocity of 0.1 m s^{-1} is 0.0042 (see equation (15.7) in

https://doi.org/10.1017/jfm.2013.523 Published online by Cambridge University Press

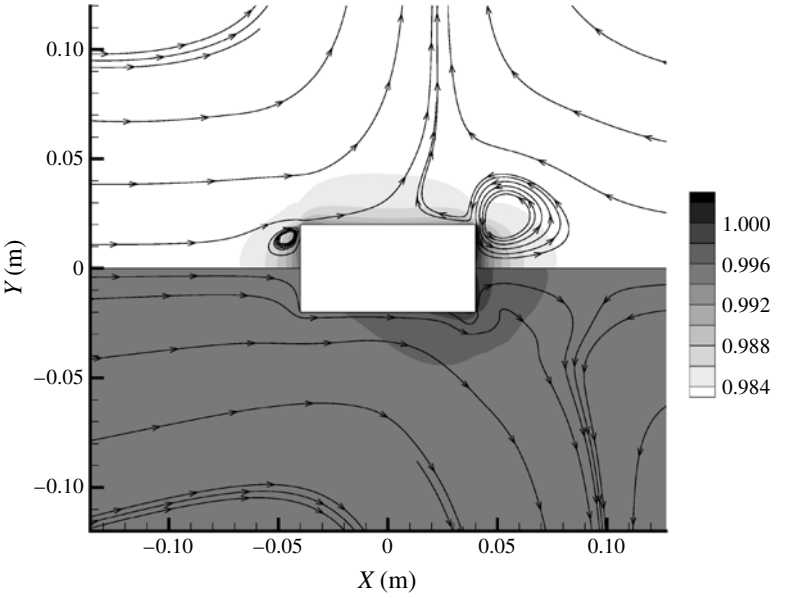


FIGURE 5. Impact of the lateral wall temperature: pressure fields and streamlines for TC1 (upper half) and TC3 (lower half); two-dimensional case, $L/D = 2$, $p_0 = 1.5$ Pa.

Bird (1994)), and thus plugging these values into the drag force expression, one may obtain $F_d = 7.4 \times 10^{-7}$ N. This is noticeably smaller than a force of 8.8×10^{-6} N produced by a pressure difference of 0.007 Pa between the hot and the cold sides of a 4 cm diameter circular vane. The pressure difference of 0.007 Pa is the smallest calculated pressure difference for a given axial coordinate, as illustrated in figure 4(*b*). Although the above force comparison is only schematic, the low flow velocities near the working sides of the vane are the likely indication that the induced bulk flow is not the governing component in the radiometric force. However, it can still dominate the shear force. Note that the pressure tends to increase from the centre to the edge of the vane, and the mechanisms driving such an increase were discussed in detail by Selden *et al.* (2009*b*) and Taguchi & Aoki (2012).

Examining the impact of the temperature condition at the vane on the flow and pressure distributions near the vane, the results for the thickest vane under consideration are shown in figure 5. Note that the pressure in the chamber is on average ∼3 % higher for TC1 than for TC3 owing to noticeably higher vane temperatures. Therefore, the pressure fields in figure 5 are normalized by the corresponding gas pressure value at the centre of the hot side of the vane. For TC3, where the cold side of the vane is kept at the chamber wall temperature, the impact of the hot side does not propagate beyond the cold edge, and the pressure at that side is fairly close to the initial pressure of 1.5 Pa, while the pressure at the hot side is approximately 0.5 % higher. For TC1, the pressure is elevated as compared to the initial value at both the cold and hot sides of the vane. It is important to note that the difference between gas pressure at the hot and cold sides for TC1 is essentially the same as for TC3. That indicates that one can expect similar pressure-based force, and any difference in radiometric force would probably be attributed to the shear component of the force and the bulk flow motion. Note that the streamlines and the entire vortex structure of TC1 and TC3 are noticeably different. In the TC3 case, the

https://doi.org/10.1017/jfm.2013.523 Published online by Cambridge University Press

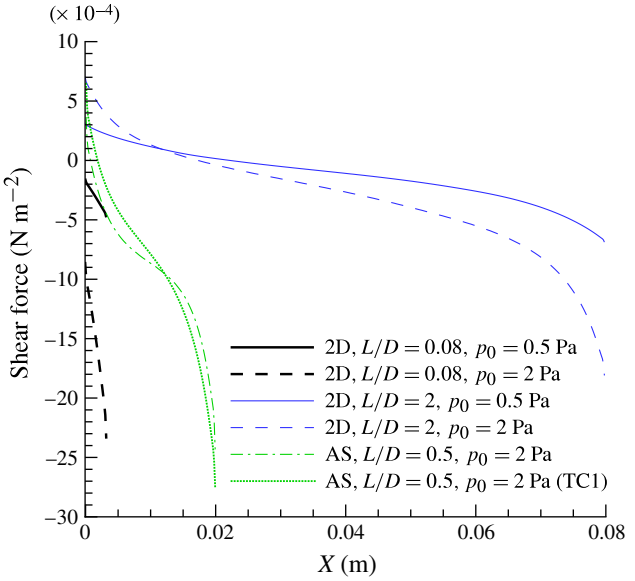


FIGURE 6. (Colour online) Distributed shear force for two-dimensional (2D) and axisymmetric (AS) vanes and different gas pressures and vane thicknesses. TC2 except where indicated.

flow is dominated by the gas moving from the cold to the hot side of the vane. The gas largely flows around the vane, with an exception of the hot edge, where there is a small vortex observed. In TC1, the flow pattern resembles that of the TC2 $L/D = 1$ case (figure 4), with two separate vortices created at the cold and hot sides of the vane and two large counter-rotating vortices formed off the lateral side of the vane. Note that the temperature gradient along the lateral side of the vane, as well as the temperature difference between the hot and the cold sides, are identical in TC2 and TC3, and thus the difference in the flow pattern is primarily due to the difference between the chamber wall and the vane temperatures. The vortex structure is therefore to a large extent formed by the flow from the cold chamber to the hot vane.

5. Radiometric force on a single vane

Quantitative evaluation of the impact of the flow motion and gas pressure differences may be conducted through the analysis of the force along the vane. The shear force distribution along the lateral side of the vane is presented in figure 6 for different pressures and vane thicknesses for both two-dimensional and AS geometries. In this figure, $X = 0$ corresponds to the cold side, and a positive force direction is the direction of the radiometric force (right to left in the previous figures). The pressures of 0.5 and 2 Pa were chosen because they bound the flow regime where the total radiometric force is at its maximum. Consider first the shear force on the thickest vane (thin solid and dashed lines in figure 6). The force values are mostly negative, indicating that the shear will decrease the total radiometric force. Note that the force is positive at the cold side, so that its direction coincides with the direction of the flow in that region (cold to hot). Similarly, the force is negative at the hot side, and thus aligned with the general flow direction there (from hot to cold).

https://doi.org/10.1017/jfm.2013.523 Published online by Cambridge University Press

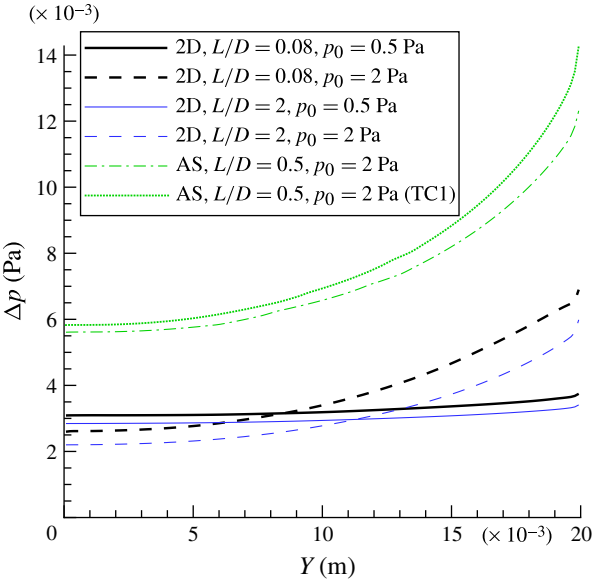


FIGURE 7. (Colour online) Distributed pressure force for two-dimensional and axisymmetric vanes and different gas pressures and vane thicknesses.

Generally, the thermal creep flow, generated by a temperature gradient along the sidewall, that moves gas from the cold side of the vane to its hot side may be expected to produce a shear force in the opposite direction, from hot to cold (conservation of momentum), and thus increase the total radiometric force. Passive shearing, produced by the cold and hot particles reflected off the working sides of the vane, may be expected to produce a shear force that coincides with the cold-to-hot flow direction. The negative shear force value that is opposite to the direction of the flow, and is present even in the absence of temperature gradients along the lateral surface, demonstrates the importance of thermal creep between the cold chamber walls and the vane surface (recall that in TC1 and TC2 both sides of the vane are at a temperature higher than the chamber wall temperature). The negative shear force is thus attributed to the dominant effect of the flow generated by the interaction of the hot vane with the cold outside chamber. There is also some impact of the gas pressure mechanism, where the force is influenced by the pressure gradients. This mechanism is expected to act in the direction of the total radiometric force. Both the bulk flow and rapid change in pressure result in steeper gradients for the higher pressure, which correspond to increasing edge effects first discussed by Einstein (1924), and then Selden *et al.* (2009*c*). For the case of a thin vane (thick solid and dashed lines), the distributed shear force is only negative, and its magnitude significantly increases with pressure. The shear force for the AS flow is qualitatively similar to the two-dimensional case. It is interesting to note that a uniform temperature gradient at the lateral wall (TC1), also shown in figure 5), is characterized by steeper force gradient than TC2, where the wall temperature linearly increases along the lateral wall. The flow velocity is somewhat higher for TC1 (not shown here), and there is also a larger difference in gas pressure near the hot and cold edges of the vane for that case, which result in a steeper force gradient.

https://doi.org/10.1017/jfm.2013.523 Published online by Cambridge University Press

The pressure force on the vertical, working side of the vane is presented in figure 7 for the same cases as in figure 6. The pressure force shown here is calculated as the difference between the pressure to the hot side and the pressure to the cold side of the vane for each of the 40 different Y stations along the vane. The coordinate $Y = 0$ corresponds to the centre of the vane, and $Y = 0.02$ m to its outer (upper) edge. Note that the pressure difference is 200–500 times smaller than the pressure force itself. This was in fact one of the main reasons behind using the deterministic solution of a model kinetic equation, instead of the DSMC method that statistically solves the Boltzmann equation. The statistical scatter associated with the DSMC method makes accurate computing of radiometric forces a prohibitively expensive problem from the computational time standpoint. As illustrated in figure 7, the effect of the vane thickness on pressure force is relatively small, and amounts to less than 10 % for a pressure of 0.5 Pa and less than 20 % for a pressure of 2 Pa, with the vane thickness increasing from $L/D = 0.08$ to $L/D = 2$. Here again, this is an indication that the pressure mechanisms, and not flow vortices, dominate the radiometric force. In all cases under consideration, the pressure force is higher to the outer edge of the vane, where pressure maxima are located. This effect increases with gas pressure, especially for the AS configuration (see Selden *et al.* (2009*b*,*c*) for a detailed discussion of area and edge mechanisms in radiometric forces).

The integral radiometric forces for most pressures p and vane thicknesses L/D considered in this work are summarized in table 1 for TC2 in two-dimensional and AS configurations. The pressure force F_p is obtained by the integration of the pressure difference such as those presented in figure 7 over the vane area. The vane area is a circular area in AS, and for two dimensions it is an equivalent area where the Z dimension is assumed to be $\pi d/4$. The shear force is obtained by the integration of the distributed shear force (see figure 6) over the lateral side of the vane, where the area in two dimensions was again assumed to be equal to that in the corresponding AS vane. The force F_t is the total radiometric force on a vane, which is the sum of the pressure and shear components. For all cases presented in the table, the maximum F_t is between 0.5 and 2 Pa.

Several conclusions can be drawn from table 1. First, the pressure force is nearly constant for the lowest pressure under consideration, where the area force is most important. For a pressure of 2 Pa, the edge force becomes more important, and the pressure force noticeably, by almost 20 %, decreases with the increasing width. The shear force is governed by the temperature difference between the cold and hot sides of the vane, as well as the chamber temperature, and, for a given gas pressure and chamber size, may be expected to peak at some large enough L/D. Second, in all cases presented here, the shear force is negative, so that it acts to reduce the total radiometric force. This is attributed primarily to the cold-to-hot bulk flow generated by the interaction of the heated vane with the cold surrounding gas and chamber walls. Third, the impact of shear (the ratio of shear to pressure force) increases with gas pressure. This is expected, since the shear force tends to zero both in the free molecular regime (gas pressure tends to zero) and in the continuum regime, and obviously has a maximum in the absolute value between those two limits. And fourth, perhaps most important, the table shows that, even for a large L/D ratio of 2, there is still significant radiometric force that exists both in two-dimensional and AS flows. The magnitude of the total radiometric force decreases by $\sim$32 % in two-dimensional and $\sim$32 % in AS flows for $L/D = 2$ as compared to an $L/D = 0.08$. Therefore, the force for the thick vane is still about two-thirds of the force on the thin vane. Since the magnitude of the shear force increases with pressure, and the shear force acts opposite

https://doi.org/10.1017/jfm.2013.523 Published online by Cambridge University Press

https://doi.org/10.1017/jfm.2013.523 Published online by Cambridge University Press

		Two-dimensional flow				Axisymmetric flow			
L/D	p (Pa)	F_p	F_s	F_t	F_s/F_p	F_p	F_s	F_t	F_s/F_p
0.08	0.5	4.09×10^{-6}	-6.66×10^{-8}	4.02×10^{-6}	-0.016	6.51×10^{-6}	-9.05×10^{-8}	6.42×10^{-6}	-0.014
	1	4.72×10^{-6}	-1.62×10^{-7}	4.55×10^{-6}	-0.034	8.91×10^{-6}	-2.62×10^{-7}	8.65×10^{-6}	-0.029
	1.5	4.84×10^{-6}	-2.47×10^{-7}	4.59×10^{-6}	-0.051	9.94×10^{-6}	-4.49×10^{-7}	9.49×10^{-6}	-0.045
	2	4.81×10^{-6}	-3.25×10^{-7}	4.45×10^{-6}	-0.068	1.04×10^{-5}	-6.33×10^{-7}	9.77×10^{-6}	-0.061
0.5	0.5	4.05×10^{-6}	-2.93×10^{-7}	3.73×10^{-6}	-0.072	6.45×10^{-6}	-3.85×10^{-7}	6.06×10^{-6}	-0.060
	1	4.68×10^{-6}	-6.62×10^{-7}	4.05×10^{-6}	-0.141	8.81×10^{-6}	-1.05×10^{-6}	7.76×10^{-6}	-0.119
	1.5	4.79×10^{-6}	-9.51×10^{-7}	3.82×10^{-6}	-0.198	9.80×10^{-6}	-1.69×10^{-6}	8.11×10^{-6}	-0.172
	2	4.76×10^{-6}	-1.17×10^{-6}	3.61×10^{-6}	-0.245	1.02×10^{-5}	-2.25×10^{-6}	7.95×10^{-6}	-0.221
1	0.5	3.97×10^{-6}	-4.61×10^{-7}	3.50×10^{-6}	-0.116	6.37×10^{-6}	-6.10×10^{-7}	5.76×10^{-6}	-0.096
	1	4.54×10^{-6}	-9.78×10^{-7}	3.55×10^{-6}	-0.215	8.65×10^{-6}	-1.59×10^{-6}	7.07×10^{-6}	-0.183
	1.5	4.60×10^{-6}	-1.32×10^{-6}	3.33×10^{-6}	-0.288	9.57×10^{-6}	-2.44×10^{-6}	7.13×10^{-6}	-0.255
	2	4.51×10^{-6}	-1.52×10^{-6}	3.00×10^{-6}	-0.337	9.90×10^{-6}	-3.13×10^{-6}	6.77×10^{-6}	-0.316
2	0.5	3.75×10^{-6}	-6.41×10^{-7}	3.11×10^{-6}	-0.171	6.24×10^{-6}	-9.25×10^{-7}	5.32×10^{-6}	-0.148
	1	4.19×10^{-6}	-1.25×10^{-6}	2.95×10^{-6}	-0.297	8.38×10^{-6}	-2.24×10^{-6}	6.14×10^{-6}	-0.268
	1.5	4.13×10^{-6}	-1.51×10^{-6}	2.62×10^{-6}	-0.366	9.17×10^{-6}	-3.28×10^{-6}	5.88×10^{-6}	-0.358
	2	3.94×10^{-6}	-1.59×10^{-6}	2.35×10^{-6}	-0.404	9.37×10^{-6}	-4.07×10^{-6}	5.30×10^{-6}	-0.434

TABLE 1. Integral radiometric forces for TC2.

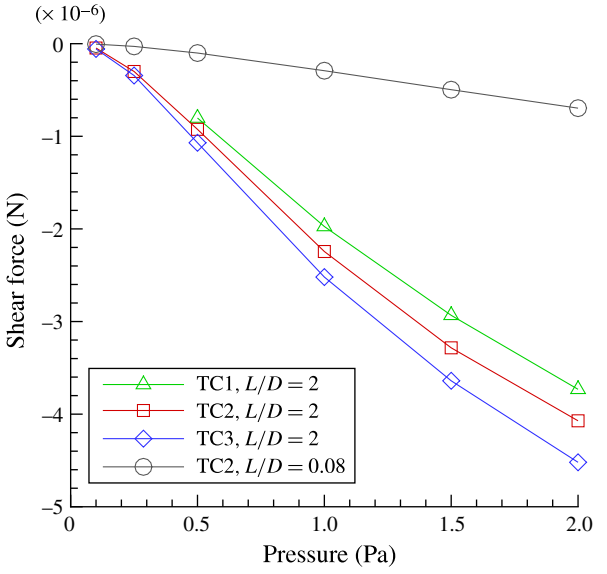


FIGURE 8. (Colour online) Integral shear force on a lateral side of a single AS vane for different temperature cases.

to the pressure force, the maximum total radiometric force shifts to lower pressures for larger L/D values. For example, for a thin axially symmetric vane, the radiometric force is maximum at $p \approx 2$ Pa, while for $L/D = 2$ the maximum shifts to $p \approx 1$ Pa.

It is important to note that the temperature difference between the hot and the cold sides of the vane, and not the temperature distribution across the vane, is the biggest factor that influences the radiometric force. Still, to some extent the force is influenced by the temperature distribution. This is illustrated in figure 8, where the shear force on an axisymmetric vane is plotted versus pressure for three temperature cases at $L/D = 2$. The thin vane case is also shown here for comparison. For all pressures under consideration, the shear force for TC2 is approximately 10 % lower than for TC1, which is explained by the stronger vortices generated by the pressure gradients along the lateral wall for TC2. The velocities in the cold to hot direction are up to 30 % higher in the vicinity of the lateral wall for TC2 as compared to TC1, which offsets the effect of the pressure gradient along that wall present in TC2 and absent in TC1. The magnitude of the shear force for TC3 is ∼10 % larger than that of TC2, again mostly due to stronger vortices in the former case. The value of the shear force is negative for all cases, which again indicates the importance of thermal creep generated by the interaction of cold chamber walls and hot sides on the radiometer vane (the thermal creep generated by the gas motion from the colder side of the vane to its hotter side, according to Newton's third law, is expected to result in a positive shear force). Note that the shear force tends to zero with decreasing pressure, and is not expected to cross zero at any pressure. The maximum total radiometric force is 7.97 μN for TC1, 6.14 μN for TC2 and 6.62 μN for TC3.

The presented results of numerical modelling are believed to be accurate solutions of the ES model kinetic equation, converged on numerical parameters such as spatial and velocity grids, and as such may provide acceptable qualitative assessment of the impact of the different factors considered in this work. However, there is always a

https://doi.org/10.1017/jfm.2013.523 Published online by Cambridge University Press

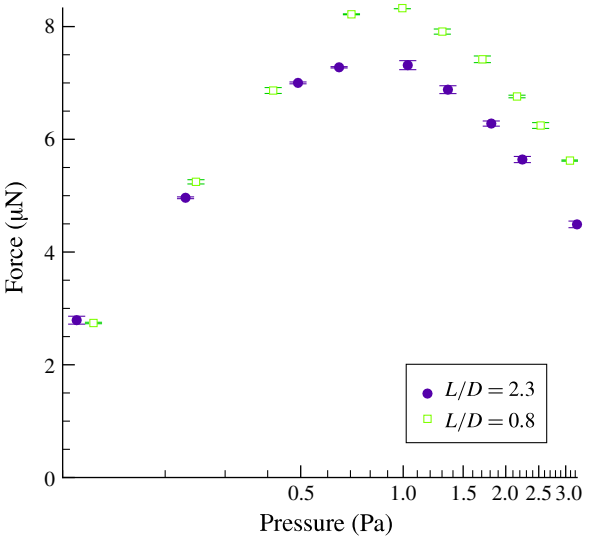


FIGURE 9. (Colour online) Experimentally measured total radiometric forces versus gas pressure for two vane thicknesses.

question of quantitative accuracy, which is related to both numerical and physical approximations. The numerical approximation pertains to how well the model equation itself reproduces the Boltzmann equation, whereas the physical approximation is related to how well the models for gas and gas–surface collisions reproduce the actual gas behaviour. The only way to evaluate those numerical and physical error bars is to compare the results with experimental data. The companion experiments were conducted for a rectangular vane, and thus carry some features of both two-dimensional and AS numerical set-ups. This makes direct comparison difficult, but still provides a valid benchmark for numerical predictions.

The experimentally measured dependence of radiometric force on gas pressure for two values of L/D is presented in figure 9. The general trend of that dependence is a bell shape with a maximum at a Knudsen number of the order of 0.1, also seen in the radiometric literature of the past. The shape is similar for the two vane geometries, although the maximum clearly shifts towards lower pressures as the thickness increases. This pattern agrees with what was observed in the computations. Moreover, the force for $L/D = 2.3$ is lower than that for $L/D = 0.8$ for pressures where the force is near its maximum. For lower pressures, corresponding to a Knudsen number of 0.5 and higher, there is virtually no dependence of force on vane thickness. Some difference between the two left-most points is related to the slight difference in the temperature gradient across the vane, and to the 5 % error bars in the temperature measurement.

Computational and experimental values of the maximum radiometric force for a given L/D ratio (those were observed at different pressures) are plotted in figure 10. The numerical results are given for two-dimensional and AS configurations. For the AS configuration, two temperature conditions at the lateral wall are shown. The numerical force predictions are proportionally adjusted to represent the same area as in the experiment (the AS numerical results were multiplied by $4/\pi$). Recall that the experimental set-up most closely corresponds to the TC1 case. Comparison of the

https://doi.org/10.1017/jfm.2013.523 Published online by Cambridge University Press

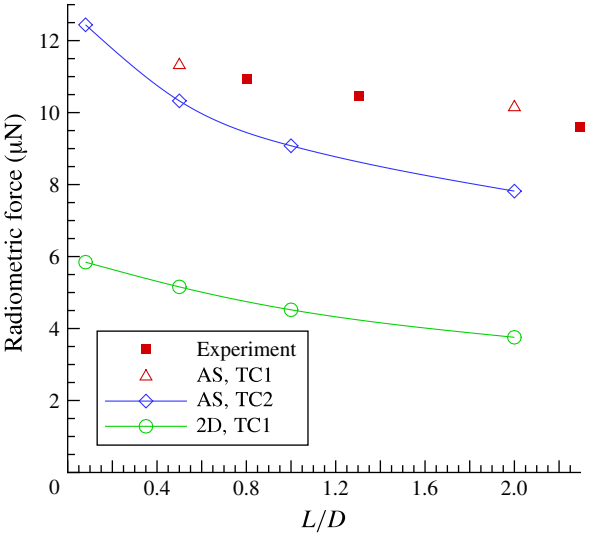


FIGURE 10. (Colour online) Maximum radiometric force for a given vane thickness: measurement and computation.

numerical AS TC1 results with the measurements demonstrates not only qualitative but also reasonable quantitative agreement. Both modelling and experiment predict fairly slow decrease of radiometric force with vane thickness; extrapolating that result to larger L/D values implies that a noticeable force may exist for the values of L/D as high as 10. The force is smaller, and the decrease with L/D is more pronounced, for TC2 (linear temperature gradient). To a large extent, this is related to the large shear force produced primarily by the vortex flow around the vane. In turn, the latter is attributed to the thermal creep cold-to-hot type flow generated by the interaction between cold walls of the chamber and hot surfaces of the vane. That interaction is much more pronounced for the two-dimensional flow than for AS flow owing to the smaller ratio of chamber to vane area in two dimensions. Thus, the dependence of the force on L/D for two-dimensional TC1 resembles that of AS TC2. The absolute force for two-dimensional flow is about two times smaller than in AS.

6. Multi-vane configuration

The single-vane results presented above demonstrate a substantial radiometric force for L/D up to two in a single-vane configuration, with the force decreasing slowly with the vane thickness. Previous research (see Cornella *et al.* 2012) has shown that one of the efficient ways to increase radiometric force for a given radiometer area is to perforate the surface of the radiometer, so that the size of the created gaps is nearly the size of the remaining surfaces (sub-vanes). The radiometric force in this case will be maximum at a Knudsen number of about 0.1, with Knudsen number now based on the size of the sub-vanes. Such a perforated configuration was found by Cornella *et al.* (2012) to be many times more efficient than the original vane for thin vanes, even though the shear force decreased the total force. In this work, the focus is on thick vanes, and the question is how much will the shear force degrade the total force when the sub-vane thickness exceeds their height.

https://doi.org/10.1017/jfm.2013.523 Published online by Cambridge University Press

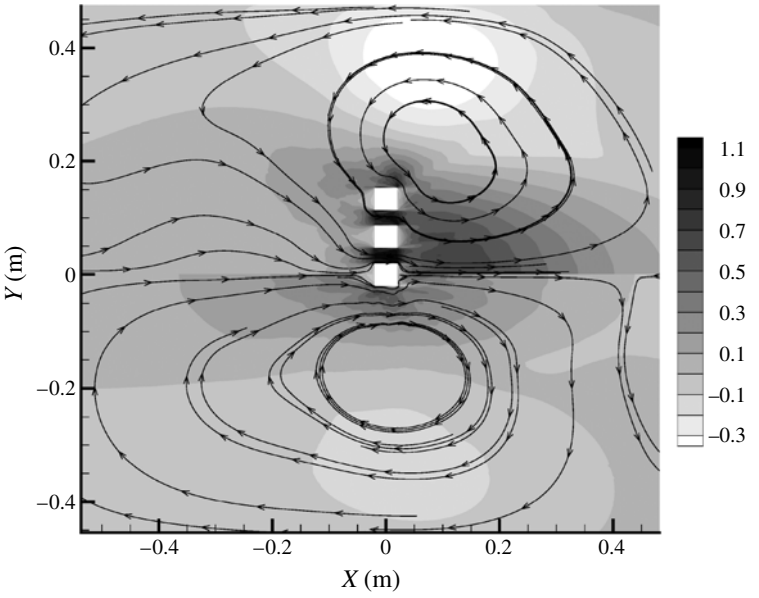


FIGURE 11. Flow velocity and streamlines for five-vane (upper half) and single-vane (lower half) configurations; $L/D = 1$, $p = 0.5$ Pa.

To this end, two-dimensional computations were conducted for a configuration with five sub-vanes (referred to below as the five-vane configuration) of a height D of 20 mm each (the same as the height of the single vanes considered earlier in this work), the gaps between sub-vanes of $0.7D$ and a thickness L, giving a range of $L/D = 0.08$ to $L/D = 2$. The TC2 temperature condition was assumed. The field of the flow velocity in the X direction and streamlines for the five-vane configuration are compared with those of a single vane in figure 11. Here, a part of the computational domain is shown in order to provide more detail of the flow in the vicinity of the vane, where $Y = 0$ is the symmetry plane. Generally, there is a fairly complex vortex flow observed for the five-vane configuration, induced by the interaction of the hot vane surfaces with the cold chamber walls. There exists a strong thermal transpiration that drives the flow through the gaps in the direction from cold to hot (left to right). The flow velocity reaches its maximum of more than 1 m s^{-1} inside the gaps. It is interesting to note that the flow near the outer vane in the five-vane configuration (0.15 m $< Y <$ 0.18 m) is qualitatively different from that for the single vane (-0.05 m $< Y < -0.02$ m in figure 11). For the multi-vane case, the flow velocity is always positive, and increases towards the hot side. For the single-vane case, the velocity is positive near the cold edge, and negative near the hot edge of the vane.

The complex vortex structure finds its place in the dependence of the total shear force of gas pressure and vane thickness. The total shear force, calculated over all lateral walls of the five sub-vanes, with the third dimension, Z, assumed to be $\pi d/4$ (similar to the single-vane force calculation of the previous section), is presented in figure 12. As before, the negative force corresponds to the positive X direction (left to right), so that the total radiometric force directed from hot to cold is positive. For a thin vane of $L/D = 0.08$, the shear force is always negative, and its magnitude

https://doi.org/10.1017/jfm.2013.523 Published online by Cambridge University Press

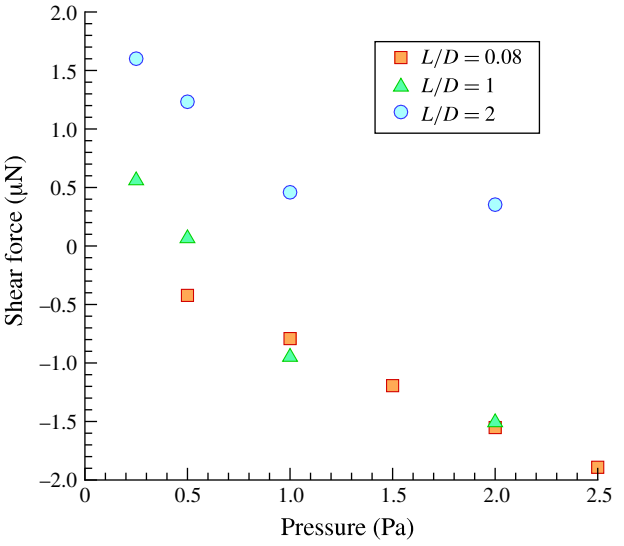


FIGURE 12. (Colour online) Integral shear force for a five-vane configuration as a function of gas pressure for different vane thicknesses.

decreases almost linearly with gas pressure, and appears to asymptote to zero for $p \to 0$. This result is in agreement with the previous findings of Cornella *et al.* (2012), where a thin multi-vane radiometer was examined in a much smaller chamber. For thicker vanes, however, there is a qualitative change in the shear force. For $L/D = 1$, the force is close to that of $L/D = 0.08$ for pressures of 1 and 2 Pa. However, for smaller pressures, it sharply increases, quickly becoming positive. Such behaviour, obviously related to the complex interplay of pressure gradients and bulk flow motion caused by the vane cold-to-hot thermal transpiration and chamber-to-vane thermal creep, is difficult if not impossible to predict theoretically. The pressure gradients are more pronounced for the multi-vane case, and thus shift the shear force more significantly towards positive values. Thermal transpiration through the gaps between the sub-vanes is, to a large extent, caused by the vane, resulting in a counter-action in the direction from hot to cold increasing the shear. Both mechanisms result in generally positive total shear at the surfaces of the internal sub-vanes. At the same time, for smaller pressures, the negative shear force on the outer side of the radiometer is reduced (see also figure 8, where a similar effect for a single vane is shown). As a result, the positive shear on the internal vanes starts to dominate and exceed the negative shear force at the outer surface driven by the bulk flow induced by the chamber–vane interaction. The pressure dependence of the shear force for $L/D = 2$ is similar to $L/D = 1$, although in the former case the shear force is positive for all pressures under consideration.

Such an effect has a noticeable impact on the radiometric force of perforated radiometers with a finite thickness. The total radiometric force, F_t, and the pressure force generated by the pressure difference between the hot and cold sides of sub-vanes are shown in figure 13. Consider first the force on the thin multi-vane radiometer ($L/D = 0.08$). The pressure force for this case peaks at ∼2.5 Pa (for a single vane, the maximum pressure force was observed at 1.5 Pa). Note that the pressure force for the five-vane configuration is less than four times larger than that for a single vane, thus

https://doi.org/10.1017/jfm.2013.523 Published online by Cambridge University Press

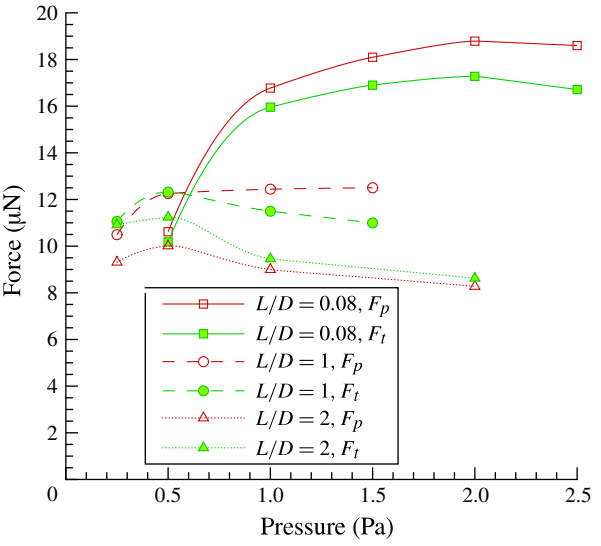


FIGURE 13. (Colour online) Pressure, F_p, and total, F_t, forces for a five-vane configuration as a function of gas pressure for different vane thicknesses.

indicating that the interference between sub-vanes noticeably impacts the force. This is also the case for the total force, which also peaks at 2.5 Pa, with a magnitude about four times larger than that of a single vane. For all pressures shown in figure 13, the shear force noticeably decreases the total force for $L/D = 0.08$. For a thick multi-vane configuration of $L/D = 2$, the maximum pressure force is observed at 0.5 Pa. For that pressure, F_p for the thin and thick vanes are close. For pressures lower than 0.5 Pa, the pressure force is higher for $L/D = 2$; for pressures higher than 0.5 Pa, the thin radiometer produces a larger pressure force.

While a smaller force for a thicker vane can be expected owing to shear force losses and generally less efficient pressure redistribution, a larger force for a thicker vane, observed for smaller pressures, is surprising. The main reason for this is believed to be the transpiration flow, which generates a large pressure gradient while driving gas from the cold side to the hot side of the vanes. Note that, even for the lowest considered pressure of 0.25 Pa, the flow is far from free molecular, with a Knudsen number based on the total radiometer height of $\sim$0.04. Comparing the maximum radiometric force for different L/D, the force decreases from over 17 μN at $L/d = 0.08$, to 12.3 μN at $L/d = 1$, to 11.2 μN at $L/d = 1$. Thus, owing to the effect of thermal transpiration and growing positive shear force, the drop in radiometric force for L/d changing from 1 to 2 is less than 10 %.

7. Conclusions

Both experimental measurements and numerical modelling, which were found to be in reasonable quantitative agreement, predict a mild decrease in radiometric force with increasing vane thickness-to-height ratio L/D. Increasing L/D fourfold from 0.5 to 2 reduces the force by 10–15 %. It is expected that noticeable radiometric force would exist on bodies as thick as $L/D = 10$. Numerical results indicate that the shear force on the lateral side of the vane acts in the direction opposite to the pressure force, and thus decreases the total radiometric force for all considered geometries and pressures.

https://doi.org/10.1017/jfm.2013.523 Published online by Cambridge University Press

The negative shear force is attributed to the bulk flow velocity associated with large vortices generated by the interaction of the cold walls of the chamber and the heated vane. The thermal creep resulting from that interaction drives the flow near the lateral side of the vane in the direction from cold to hot, the same as the direction of the shear force on the lateral side of the vane. The effect of the flow induced by chamber walls is expected to be more pronounced in the two-dimensional case. The observed two-dimensional flow structure, characterized by a small vortex observed in front of the colder side of the vane, and a larger size vortex surrounding the rest of the vane (see insets in figure 3), is expected to exist through the entire transitional flow regime. In the near-continuum flow, where the mean free path becomes significantly smaller than the vane size, one can expect the transformation of such flow structure to a one-vortex flow, similar to that qualitatively discussed by Kennard (1938). The transformation may indicate that the chamber–vane interaction becomes less significant, owing to shorter relaxation lengths, than the thermal creep between the sides of the vane.

Comparing the three temperature regimes examined in this work, it was found that the magnitude of the shear force increases by $\sim$10 % from case 1 (the hot and the cold side temperatures $T_h = 403$ K and $T_c = 378$ K, respectively, and the lateral wall kept at T_c) to case 2 (linear T gradient along the lateral wall), and also from case 2 to case 3 ($T_h = 325$ K and $T_c = 300$ K, with linear gradient along the lateral wall). The maximum total radiometric force was observed for case 1.

Computations were also conducted for a multi-vane two-dimensional configuration, where five vanes of a height of 40 mm each and separated by 28 mm created a radiometer with a total height of 312 mm. The thickness of the radiometer was varied from 3.2 to 80 mm. It was found that, owing to significant transpiration through the gaps at lower pressures, driven by the interaction between the cold and hot sides of the vane, the shear force becomes positive, and works to counteract the vane-generated transpiration flow. Transpiration also results in increasing pressure gradient between the hot and cold sides of the vane, mostly noticeable for Knudsen numbers of 0.02 and higher. The total radiometric force for a multi-vane geometry decreases by less than 10 % for the vane thickness increasing from $L/D = 1$ to $L/D = 2$, similar to what was obtained for a single-vane configuration. All this indicates that a considerable radiometric force is expected for thick single- and multi-vane geometries even when the vane thickness many times exceeds their height.

Acknowledgements

The work was supported in part by the Air Force Office of Scientific Research (Dr M. Birkan). The modelling effort used, in part, the Extreme Science and Engineering Discovery Environment (XSEDE), which is supported by National Science Foundation grant number OCI-1053575.

REFERENCES

BIRD, G. A. 1994 *Molecular Gas Dynamics and the Direct Simulation of Gas Flows*. Clarendon.

BRÜCHE, E. & LITTWIN, W. 1928 Experimental contributions to the radiometer question. *Z. Phys.* **52**, 318–335.

CLIFT, R., GRACE, J. R. & WEBER, M. E. 1978 *Bubbles, Drops, and Particles*. Academic Press.

CORNELLA, B., KETSDEVER, A., GIMELSHEIN, N. & GIMELSHEIN, S. 2012 Analysis of multi-vane radiometer arrays in high-altitude propulsion. *J. Propul. Power* **28** (4), 831–839.

https://doi.org/10.1017/jfm.2013.523 Published online by Cambridge University Press

CROOKES, W. 1874 On attraction and repulsion resulting from radiation. *Phil. Trans. R. Soc. Lond.* **164**, 501–527.

CZERNY, M. & HETTNER, G. 1924 The measurement of the thermal slip of gases. *Z. Phys.* **30**, 258–267.

EINSTEIN, A. 1924 Zur theorie der radiometerkräfte. *Z. Phys.* **27**, 1–6.

GIMELSHEIN, N., GIMELSHEIN, S., SELDEN, N. & KETSDEVER, A. 2010 Modelling of low-speed rarefied gas flows using a combined ES-BGK/DSMC approach. *Vacuum* **85** (2), 115–119.

HOLWAY, L. H. 1966 Numerical solutions for the BGK-model with velocity dependent collision frequency. In *Proceedings of Fourth International Symposium on Rarefied Gas Dynamics, University of Toronto, 1964*, pp. 193–215. Academic Press.

JAMISON, A. J., KETSDEVER, A. D. & MUNTZ, E. P. 2002 Gas dynamic calibration of a nano-newton thrust stand. *Rev. Sci. Instrum.* **73** (10), 3629–3637.

KENNARD, E. H. 1938 *Kinetic Theory of Gases*. McGraw-Hill.

MARSH, H. E. 1926 Further experiments on the theory of the vane radiometer. *J. Opt. Soc. Am.* **12**, 135–148.

MAXWELL, J. C. 1879 On stresses in rarified gases arising from inequalities of temperature. *Phil. Trans. R. Soc. Lond.* **170**, 231–256.

MIEUSSENS, L. 2000 Discrete-velocity models and numerical schemes for the Boltzmann–BGK equation in plane and axisymmetric geometries. *J. Comput. Phys.* **162** (2), 429–466.

REYNOLDS, O. 1874 On forces caused by evaporation from, and condensation on, a surface. *Proc. R. Soc. Lond.* **22**, 401–407.

REYNOLDS, O. 1876 On the forces caused by the communication of heat between a surface and a gas; and on a new photometer. *Phil. Trans. R. Soc. Lond.* **166**, 725–735.

SCANDURRA, M., IACOPETTI, F. & COLONA, P. 2007 Gas kinetic forces on thin plates in the presence of thermal gradients. *Phys. Rev.* E **75**, 026308.

SELDEN, N., GIMELSHEIN, N., GIMELSHEIN, S. & KETSDEVER, A. 2009*a* Analysis of accommodation coefficients of noble gases on aluminum surface with an experimental/computational method. *Phys. Fluids* **21** (7), 073108.

SELDEN, N. P. & KETSDEVER, A. D. 2003 Comparison of force balance calibration techniques for the nano-newton range. *Rev. Sci. Instrum.* **74**, 5249–5254.

SELDEN, N., NGALANDE, C., GIMELSHEIN, N., GIMELSHEIN, S. & KETSDEVER, A. 2009*b* Origins of radiometric forces on a circular vane with a temperature gradient. *J. Fluid Mech.* **634**, 419–431.

SELDEN, N., NGALANDE, C., GIMELSHEIN, S., MUNTZ, E. P., ALEXEENKO, A. & KETSDEVER, A. 2009*c* Area and edge effects in radiometric forces. *Phys. Rev.* E **79**, 041201.

SEXL, T. 1926 The theory of radiometer effects II. *Ann. Phys.* **81** (24), 800–806.

TAGUCHI, S. & AOKI, K. 2012 Rarefied gas flow around a sharp edge induced by a temperature field. *J. Fluid Mech.* **694**, 191–224.

TCHEREMISSINE, F. G. 1996 The conservative discrete ordinates method for solving of Boltzmann kinetic equation. In *Proceedings of International Symposium on Rarefied Gas Dynamics* (ed. C. Shen), pp. 297–302. Peking University Press.

YOUNG, J. B. 2011 Thermophoresis of a spherical particle: reassessment, clarification and new analysis. *Aerosol Sci. Technol.* **45**, 927–948.

https://doi.org/10.1017/jfm.2013.523 Published online by Cambridge University Press